# Hybrid Monte Carlo—fluid model for a microsecond pulsed glow discharge

JAAS

Full Paper

**Annemie Bogaerts* and Renaat Gijbels**

*University of Antwerp, Department of Chemistry, Universiteitsplein 1, B-2610 Wilrijk-Antwerp, Belgium. E-mail: bogaerts@uia.ua.ac.be*

***Received 27th April 2000, Accepted 12th June 2000***
***Published on the Web 26th July 2000***

A hybrid model is developed for a microsecond pulsed analytical glow discharge. It consists of a Monte Carlo model for the fast electrons, a fluid model for the slow electrons and argon ions, coupled to Poisson's equation for the electric field calculation, and a Monte Carlo model for the fast argon ions and atoms in the cathode dark space (CDS). Typical results of this model include the electrical characteristics (*i.e.*, potential, current, power, as well as the gas temperature), the electric potential distributions, the argon ion density profiles, and the rates of various ionization and recombination mechanisms. These results are presented as a function of time during and after the pulse. Comparison with experimental data has been made for the electrical characteristics (for which experimental data were available), and good agreement has been reached. This suggests that the other calculated quantities, for which no experimental data are available, are also correctly predicted in the model.

## 1. Introduction

In recent years, there has been a growing interest in pulsed glow discharges, used as analytical sources for mass spectrometry (GDMS), optical emission spectrometry (GD-OES), atomic absorption and fluorescence spectrometry (GD-AAS and GD-AFS).[1–50] The main advantages are a higher peak power during the pulse, and hence higher analyte signals for the same average power as in conventional direct current (dc) discharges; as well as a reduction of background signals when time-resolved detection is applied (since analyte and background species appear to be formed at different times in or after the pulse). The pioneering work in the field of pulsed analytical glow discharges, mainly in hollow cathode sources, goes back several decades in history,[1–14] but it received new and wider attention about 10 years ago, mainly from Harrison and Winefordner and coworkers.[15–17] They found higher sputter yields and ion signal intensities compared to dc glow discharge sources,[15] and when laser excited fluorescence was measured in the "dark period" between pulses, signals with reduced background noise were obtained.[16] Moreover, they investigated the ionization mechanisms and the pre- and after-peaks of ion signals, as well as their potential analytical use, in millisecond pulsed glow discharges.[15,17] Around the same time, Chakrabarti *et al.* used millisecond pulsed glow discharge sputtering for atomic absorption spectrometry.[18] A few years later, King and Pan[19-21] made use of optical emission, atomic absorption and mass spectrometry to measure temporal profiles of various atomic and ionic species in millisecond pulsed glow discharges, to obtain a better insight into the ionization and excitation mechanisms of sputtered atoms after termination of the pulse.

Other work in millisecond pulsed discharges dealt with the study of rare earth oxide equilibria in pulsed GDMS,[22] the improvement of the signal to noise (S/N) ratio in glow discharge ion trap mass spectrometry by synchronizing the pulsed voltage with the ion injection (during pulse "on") and the data acquisition (during pulse "off"),[23] the discrimination against isobaric interferences (*e.g.*, determination of Ca in Ar) by time-gated detection (since the analyte and discharge gas ions are formed at different times),[24,25] and the combination of a laser ablation system with a pulsed glow discharge.[26] However, in recent years, focus has been shifted toward microsecond pulsed glow discharges. A large number of papers on this topic have been published in the last four years by Harrison's group.[27–41] In the microsecond pulsed regime, still higher peak voltages and currents can be applied for the same average power, leading to even higher analyte signals, compared to the millisecond pulsed regime and to dc and rf discharges.[27,30] This high instantaneous power during the short (microseconds) pulse, turns the normally observed blue glow of an argon glow discharge into a distinctive green, due to the significant population of highly excited copper atomic states.[31] The microsecond pulsed glow discharge has been coupled by Harrison and coworkers to atomic emission, absorption and fluorescence spectroscopy, as well as mass spectrometry (*e.g.*, ref. 32). Time-resolved emission and absorption spectroscopy have been applied to study the atomization, excitation and ionization mechanisms in the microsecond pulsed discharge.[33] In ref. 34, a microsecond pulsed hollow cathode discharge, combined with a gated detection system, yielded optical emission intensities that were 3–4 orders of magnitude higher than in conventional dc hollow cathode sources. The combination of a pulsed laser ablation system with microsecond pulsed glow discharges has also been presented.[35,36] Recently, the group also applied the microsecond pulsed operation mode to a Grimm-type source, both for optical emission and mass spectrometry.[37–40] Finally, from the coupling of the microsecond pulsed glow discharge to a time-of-flight mass spectrometer (μs-pulsed GD-TOF-MS), promising results can be expected.[31,41] Indeed, the temporal advantage inherent in the combination of a pulsed source and a pulsed mass analyzer permits strong discrimination against discharge gas interferences. In addition, because the TOF mass spectrometer is able to operate at a high repetition rate, a large number of spectra can be acquired and averaged in a short period of time, resulting in a significant enhancement in S/N ratio.[31,41]

The coupling of a microsecond pulsed glow discharge with a TOF mass spectrometer has also successfully been achieved by a group in China.[42–45] They reported very high transient sputtering rates and hence high signal intensities, but the average sputtering rate is rather low, which makes the technique potentially useful in the field of surface analysis. It

was found that the sputtered surface obtained with a μs-pulsed glow discharge was much finer than that of a dc glow discharge, and had minimum crater effects.[42–45]

Finally, a recent collaboration between Majidi *et al.* and King's group led to a number of interesting publications about milli- and microsecond pulsed glow discharges. They used atomic emission, absorption and laser induced fluorescence to perform temporally and spatially resolved diagnostics of both milli- and microsecond pulsed glow discharges.[46] Moreover, they applied milli- and microsecond pulsed GD-TOF-MS for the concurrent acquisition of structural, molecular and elemental information of samples.[47–50] Indeed, depending on the extent of interaction with the plasma, the samples may undergo soft chemical ionization yielding molecular ions or they may be completely atomized and ionized yielding elemental information.

To understand the underlying plasma processes in pulsed glow discharges, both during the pulse and in the afterglow, we have developed a 2D hybrid model to describe the behavior of electrons, argon ions and argon atoms. It is based on a Monte Carlo model for the fast electrons, a fluid model for the slow electrons and argon ions, including the Poisson equation for a self-consistent electric field, as well as a Monte Carlo model for the argon ions and fast argon atoms in the cathode dark space (CDS). This model is similar to the models we have developed previously for dc[51,52] and rf[53,54] discharges, although the pulsed operation mode requires a somewhat specific approach (see below).

There are a few models in the literature for pulsed discharges, albeit not analytical glow discharges (*e.g.*, refs. 55–58). In ref. 55, a 1D fluid model for electrons and argon ions is developed to simulate the creation process of the electrons and ions in a μs-pulsed discharge, with 100 μs pulse duration and 50 Hz pulse repetition frequency (PRF). However, the discharge cell under consideration is much larger than typical analytical glow discharge cells (*i.e.*, 25 cm long and 4 cm diameter). Moreover, the model is applied to lower voltages and pressures (*i.e.*, $V = 800$–$1000$ V; $p = 0.3$–$0.75$ Torr), hence yielding much lower plasma densities (order of $10^{10}$ cm$^{-3}$ compared to $\approx 10^{14}$ cm$^{-3}$ at the conditions under study here; see below). In ref. 56, a 2D hybrid Monte Carlo–fluid model (more or less similar to our approach) has been applied to describe the initiation phase of pseudospark discharges. The latter are a kind of pulsed discharge in a hollow cathode geometry, characterized by an extremely rapid transition, often accompanied by a high-brightness electron beam, to a relatively long-lived, high current density diffuse discharge. They are used for the switching of high currents or in applications which require an intense electron beam source. The applied voltage can be tens of kV, yielding currents of several tens of kA in a very short time (*i.e.*, several tens or hundreds of nanoseconds); hence the discharge conditions are much more extreme than in analytical discharges. In ref. 57, a 1D particle-in-cell (PIC) model was developed for a pulsed (order of 1 ms) rf discharge in argon; the pressure, however, was much lower (*i.e.*, order of 50 mTorr) than for our conditions. Finally, a 2D fluid model and PIC model are described in ref. 58 for an ac plasma display cell. Such a cell is extremely small (*e.g.*, width of 1260 μm and distance between the electrodes of 160 μm), and the pressure is very high (*e.g.*, 500 Torr, in a mixture of 90% neon and 10% xenon). Hence, these models apply to completely different types of discharges and operating conditions, compared to the analytical pulsed glow discharge conditions (see Section 3). Very recently, a model has been presented for a pulsed analytical glow discharge,[59] using a similar approach as in our models. The conditions under study (*i.e.*, 800 V discharge voltage, 1 A current and 1 Torr argon gas pressure) are of the same order of magnitude as the conditions of interest in the present work. However, the results presented up to now are only very limited and they do not reveal a very detailed picture of the pulsed analytical glow discharge.[59]

In the following, we will describe our hybrid model set-up and show some results for a μs-pulsed glow discharge, with emphasis on the time-dependence of the electrical characteristics, the plasma densities and the ionization and recombination processes in the plasma.

## 2. Description of the models

The present hybrid model focuses on the electrical characteristics in the μs-pulsed glow discharge. Hence the plasma species considered in the model are argon atoms, argon ions and electrons. Argon atoms in excited levels (including the metastables) and sputtered atoms and ions are not yet incorporated, since we calculated with our previous models for dc and rf discharges that they do not play a significant role in determining the electrical characteristics (contribution of less than 1%),[60,61] at least for dc and rf discharges. However, we have also found that the role of sputtered atoms and ions increases at higher electrical powers, and, since μs-pulsed discharges operate at much higher instantaneous powers than dc and rf discharges, it might well be possible that these species play a non-negligible or even dominant role in the pulsed mode. Hence, it should be realized that neglecting these species is a limitation of the present model. In the near future, we plan to extend our model to the incorporation of argon excited atoms (including the metastables) and sputtered atoms and ions, in analogy to our dc and rf models, so that we can obtain a better feeling about the importance of these species in the model.

The three sub-models for electrons, argon ions and fast argon atoms in the hybrid model network are explained below in some more detail.

### 2.1. Monte Carlo model for the fast electrons

The Monte Carlo model describes the behavior of the individual electrons in the plasma, *i.e.*, their movement under the influence of the electric field, and their collisions with gas atoms. By following a large number of individual electrons as a function of time during and after the pulse, their behavior is simulated in the most accurate way. The Monte Carlo solver starts at $t = 0$, which is the start of the pulse. During successive time-steps, of the order of $10^{-12}$–$10^{-11}$ s ($= 10^{-6}$–$10^{-5}$ μs) in the pulse and $10^{-10}$–$10^{-8}$ s ($= 10^{-4}$–$10^{-2}$ μs) in the afterglow, a number of electrons are followed one after the other. The electrons start at the cathode, determined by the ion flux bombarding the cathode (calculated as a function of time in the fluid model; see below) and the secondary electron emission coefficient. Their trajectory during one time-step, $\Delta t$, is calculated by Newton's laws:

$$z = z_0 + v_{z_0}\Delta t + \frac{q\,E_{\mathrm{ax}}(z,\,r,\,t)}{2m}(\Delta t)^2$$

$$x = x_0 + v_{x_0}\Delta t + \frac{q\,E_{\mathrm{rad}}(z,\,r,\,t)\,\cos(\alpha)}{2m}(\Delta t)^2$$

$$y = y_0 + v_{y_0}\Delta t + \frac{q\,E_{\mathrm{rad}}(z,\,r,\,t)\,\sin(\alpha)}{2m}(\Delta t)^2$$

$$v_z = v_{z_0} + \frac{q\,E_{\mathrm{ax}}(z,\,r,\,t)}{m}\Delta t$$

$$v_x = v_{x_0} + \frac{q\,E_{\mathrm{rad}}(z,\,r,\,t)\,\cos(\alpha)}{m}\Delta t$$

$$v_y = v_{y_0} + \frac{q\,E_{\mathrm{rad}}(z,\,r,\,t)\,\sin(\alpha)}{m}\Delta t$$

where $z_0$, $x_0$, $y_0$ and $z$, $x$, $y$ are the position coordinates before

and after $\Delta t$, $v_{z_0}$, $v_{x_0}$, $v_{y_0}$, $v_z$, $v_x$, $v_y$ are the velocities before and after $\Delta t$, $E_{ax}$ and $E_{rad}$ are the axial and radial electric field as a function of axial and radial position and time (obtained from the fluid model,see below), $\alpha$ is the azimuthal angle of the radial position (*i.e.*, the angle of the radial position coordinates with respect to the $x$-axis), and $q$ and $m$ are the electron charge and mass, respectively.

The new position coordinates ($z$, $x$, $y$) determine whether the electron reaches the cell walls or not. If the electron collides at the walls, it can be reflected, cause secondary electron emission or become absorbed, defined by reflection and secondary electron emission coefficients and random numbers (for detailed information, see ref. 51).

However, if the electron does not collide at the walls (which is indeed mostly the case), the probability for collision of this electron during the time-step $\Delta t$ is calculated and compared with a random number between 0 and 1:

$$Prob_{coll} = 1 - \exp\{-\Delta s \Sigma[n\sigma_{coll}(E)]\}$$

where $\Delta s$ is the distance traveled during $\Delta t$; $n$ and $\sigma_{coll}(E)$ are the densities of the target particles and the cross sections of the different collision types of the electron with energy $E$. The collisions taken into account in this Monte Carlo model, are electron impact excitation and ionization of the argon gas atoms, as well as elastic momentum transfer with the argon atoms. The cross sections for these collisions are adopted from Phelps.[62]

If the collision probability is lower than the random number, no collision occurs, and the Monte Carlo solver continues with the next electron. If the collision probability is higher than the random number, a collision takes place.

To determine which collision takes place, the partial collision probabilities of the individual collision processes (*i.e.*, $P_{exc,Ar}$; $P_{ion,Ar}$; and $P_{ela,Ar}$) are calculated, by dividing the individual cross sections by the total collision cross section:

$$\sigma_{tot} = \sigma_{exc,\,Ar} + \sigma_{ion,\,Ar} + \sigma_{ela,\,Ar}$$

$$P_{exc,\,Ar} = \frac{\sigma_{exc,\,Ar}}{\sigma_{tot}}, \quad P_{ion,\,Ar} = \frac{\sigma_{ion,\,Ar}}{\sigma_{tot}}, \quad P_{ela,\,Ar} = \frac{\sigma_{ela,\,Ar}}{\sigma_{tot}}$$

Hence, the sum of the partial collision probabilities is equal to one. Then, a second random number ($rn$) is generated and compared with the partial collision probabilities:

if $rn \leqslant P_{exc,Ar}$, an excitation collision occurs;

if $P_{exc,Ar} < rn \leqslant P_{exc,Ar} + P_{ion,Ar}$, an ionization collision occurs; and

if $P_{exc,Ar} + P_{ion,Ar} < rn \leqslant P_{exc,Ar} + P_{ion,Ar} + P_{ela,Ar}$, an elastic collision takes place.

Depending on the kind of collision, the new energy and direction after collision are determined, based on scattering formulas and some more random numbers, according to the published procedure.[53,63]

Then, the Monte Carlo solver moves to the next electron, which will be described in the same way, until all electrons are followed during that time-step. Subsequently, the model proceeds with the next time-step, to follow all the electrons again in a similar way, *i.e.*, the continuation of the behavior of electrons from the previous time-step, as well as new electrons starting at the cathode by secondary electron emission, and new electrons created in the plasma by an ionization collision during the previous time-step.

Electrons can also become lost in the Monte Carlo model, *i.e.*, when they are absorbed at the cell walls (see above), or when their energy is lower than the threshold for inelastic collisions, which is defined here as 11.55 eV (*i.e.*, the excitation energy for argon atoms). Indeed, when the electrons have lower energy, their primary role is to contribute to the electric current and the negative space charge. This can as well be simulated, and much faster, in a fluid model (see below). Hence, the electrons with energy lower than 11.55 eV are transferred to the slow electron group, to be described in the fluid model (see below).

This procedure of following a large number of individual electrons during successive time-steps is repeated till the end of the afterglow time after the pulse, *i.e.*, just before the next pulse would start. Indeed, the model simulates only one pulse+afterglow, because at the end of the afterglow, the plasma is extinguished again at the conditions under study (10 μs-pulse with 200 Hz repetition frequency). Hence, the behavior of the electrons in the next pulse would be exactly the same, *i.e.*, periodic steady state is reached over one pulse+afterglow period.

### 2.2. Fluid model for the slow electrons and argon ions

The slow electrons, which have been transferred from the Monte Carlo model (see above), are described, together with the argon ions, with the continuity equations and the transport equations, based on diffusion and on migration in the electric field:

$$\frac{\partial n_{Ar^+}(z,\,r,\,t)}{\partial t} + \overline{\nabla}\cdot\overline{j_{Ar^+}}(z,\,r,\,t) = R_{Ar^+}(z,\,r,\,t) - R_{3Brec(e)}(z,\,r,\,t) - R_{3Brec(Ar)}(z,\,r,\,t) - R_{rad.rec}(z,\,r,\,t)$$

$$\frac{\partial n_e(z,\,r,\,t)}{\partial t} + \overline{\nabla}\cdot\overline{j_e}(z,\,r,\,t) = R_e(z,\,r,\,t) - 2\times R_{3Brec(e)}(z,\,r,\,t) - R_{3Brec(Ar)}(z,\,r,\,t) - R_{rad.rec}(z,\,r,\,t)$$

$$\overline{j_{Ar^+}}(z,\,r,\,t) = \mu_{Ar^+} n_{Ar^+}(z,\,r,\,t)\overline{E}(z,\,r,\,t) - D_{Ar^+}\overline{\nabla} n_{Ar^+}(z,\,r,\,t)$$

$$\overline{j_e}(z,\,r,\,t) = -\mu_e n_e(z,\,r,\,t)\overline{E}(z,\,r,\,t) - D_e\overline{\nabla} n_e(z,\,r,\,t)$$

$n_{Ar^+}$ and $n_e$ are the argon ion and electron densities; and $\overline{j_{Ar^+}}$ and $\overline{j_e}$ are the corresponding fluxes (in vector notation). $R_{Ar^+}$ and $R_e$ are the creation rates of argon ions and electrons, which result from the Monte Carlo model (*i.e.*, $R_{Ar^+}$ is the rate of electron impact ionization, and $R_e$ is the rate of transfer to the slow electron group).

Beside ionization (*i.e.*, creation of electrons and ions) also electron–ion recombination (*i.e.*, destruction of electrons and ions) is taken into account in the model. From the conservation laws of momentum and energy, it follows that a simple two-body coalescence is not allowed.[64] However, some alternative recombination processes can occur, *i.e.*:

(1) three-body recombination (in which a third body, either an electron or a gas atom or even the cell wall, takes part in the collision process, taking away the excess energy and allowing to satisfy the conservation laws);
(2) radiative recombination (in which the excess energy is carried away by a photon);
(3) dissociative recombination (for molecular ions; a two-body recombination is now possible, since the collision product can dissociate and the recombination energy is converted into kinetic and potential energy of the dissociation products); and
(4) two-stage recombination (forming an intermediate negative ion, but this is very unlikely for argon).

For argon, only three-body recombination and radiative recombination come into play.

$R_{3Brec(e)}$ is the three-body recombination rate where the third body is an electron (*i.e.*, $Ar^+ + e^- + e^- \rightarrow Ar + e^-$); $R_{3Brec(e)} = k_{3Brec(e)}(n_e)^2(n_{Ar^+})$ with $k_{3Brec(e)} = 10^{-24}\,cm^6\,s^{-1}$ (refs. 65, 66). $R_{3Brec(Ar)}$ is the three-body recombination rate with the third body being an argon gas atom (*i.e.*, $Ar^+ + e^- + Ar \rightarrow Ar + Ar$); $R_{3Brec(e)} = k_{3Brec(e)}(n_e)(n_{Ar^+})$, with $k_{3Brec(Ar)} = 10^{-11}\times p\,cm^3\,s^{-1}$ (where $p$ is the gas pressure in Torr)

(ref. 67). $R_{rad.rec}$ is the radiative recombination rate (*i.e.*, $Ar^+ + e^- \rightarrow Ar + h\nu$); $R_{rad.rec} = k_{rad.rec}(n_e)(n_{Ar^+})$, with $k_{rad.rec} = 10^{-11}$ cm$^3$ s$^{-1}$ (ref. 68).

Further, $\bar{E}$ is the electric field; and $D_{Ar^+}$, $D_e$, $\mu_{Ar^+}$ and $\mu_e$ are the argon ion and electron diffusion coefficients and mobilities, respectively. Their numerical values are taken to be:[69] $D_{Ar^+} = 40$ cm$^2$ s$^{-1}$, $D_e = 1.2 \times 10^6$ cm$^2$ s$^{-1}$, $\mu_e = 3 \times 10^5$ cm$^2$ s$^{-1}$ V$^{-1}$, $\mu_{Ar^+} = 1500$ cm$^2$ s$^{-1}$ V$^{-1}$ at 1 Torr and 298 K.

These four equations are coupled to Poisson's equation, to obtain a self-consistent electric field distribution:

$$\nabla^2 V(z, r, t) + \frac{e}{\varepsilon_0}[n_{Ar^+}(z, r, t) - n_e(z, r, t)] = 0; \; \bar{E} = -\bar{\nabla} V$$

where $V$ is the electric potential and $\varepsilon_0$ is the permittivity in vacuum.

Solving these coupled differential equations is a difficult numerical task. The method we used is based on the Scharfetter-Gummel exponential scheme.[51,69–72] The basic idea is that the particle fluxes are assumed to be constant between mesh points instead of the densities. The advantage of this scheme is its ability to switch between situations where either the migration component or the diffusion component of the particle flux is dominant [*i.e.*, high and low electric field, cathode dark space (CDS) and negative glow (NG), respectively].

The equations are solved as a function of time during one pulse+corresponding afterglow. The time-step was typically $10^{-10}$ s during the pulse (which presents the most severe conditions, and hence largest probability for instability problems in the model), and much larger in the afterglow, *i.e.*, typically $5 \times 10^{-10}$ s in the beginning of the afterglow and gradually increasing toward $10^{-6}$ s at the end of the afterglow. Moreover, within each time-step, the equations were solved for several substeps (up to 3000) until a smooth solution was reached, before moving to the next time-step.

### 2.3. Monte Carlo model for the argon ions and fast argon atoms in the CDS

The above fluid approach is in principle much faster than the Monte Carlo method, but it is only valid for "slow" plasma species, which are more or less in equilibrium with the electric field; this means that the energy they gain from the electric field is more or less balanced by the energy they lose due to collisions. Since the argon ions are not really in equilibrium with the strong electric field in the CDS, we use not only a fluid approach, but also the more accurate Monte Carlo method to describe the argon ions in this region. Moreover, the fast argon atoms, created from elastic collisions of the argon ions with background gas atoms, are also simulated with a Monte Carlo approach in the CDS.

The procedure of this ion and fast atom Monte Carlo model is very similar to the electron Monte Carlo model, and will therefore not be explained in detail anymore. The collision processes taken into account in this model are fast argon ion and atom impact ionization and excitation of the argon gas, as well as elastic collisions with the argon gas atoms. For the ions, the elastic collisions also comprise symmetric charge transfer with argon atoms, which is treated as an elastic collision with backward scattering.[73] The collision cross sections are all adopted from Phelps.[73,74]

When the fast argon ions or atoms give rise to an ionization collision, a new ion and electron are created. The ions are also followed in this Monte Carlo model, and the electrons are stored in an array. When the argon ion and atom Monte Carlo model is completely finished, the electrons created in this model are also followed with a Monte Carlo model, similarly to the one described in 2.1 (see also below).

The ion and atom Monte Carlo model is continued, for all individual ions and atoms, during successive time-steps until the end of the afterglow is reached, like in the electron Monte Carlo model. Again, some ions and atoms can be lost from the model before the end of the afterglow is reached, *i.e.*, when the ions arrive at the cell walls (where they will be neutralized), and when the atoms become thermalized, after collisions in the plasma or at the cell walls.

### 2.4. Coupling of the three submodels

The two Monte Carlo models and the fluid model are run iteratively, until convergence is reached. First, the fluid equations are solved, assuming arbitrary values for the ion and slow electron creation rates. The results of this fluid model are, among others, the electric field as a function of time and (axial and radial) position, as well as the argon ion flux bombarding the cathode and the ion flux entering the CDS, both as a function of radial position and time. These values are used in the Monte Carlo models.

From the ion flux bombarding the cathode, multiplied with the ion-induced secondary electron emission coefficient (taken as 0.083 for argon bombardment of a copper cathode[75]), the electron flux starting at the cathode as a function of time and radial position is obtained. Moreover, the electric field from the fluid model determines the trajectory of the electrons in the Monte Carlo model. The electron Monte Carlo model yields, among others, the ionization rate of argon by electron impact (*i.e.*, the creation rate of argon ions), as a function of time and (axial and radial) position.

The latter is used in the argon ion and fast atom Monte Carlo model, to determine the number of argon ions created in the CDS. Moreover, the argon ion flux entering the CDS from the NG, as a function of time and radial position, is taken from the fluid model (see above). Outputs of the argon ion and fast atom Monte Carlo model are, for instance, the argon ion and atom impact ionization rates (*i.e.*, the creation rates of new electrons).

Next, the fast electron Monte Carlo model is calculated again, incorporating these new electrons formed by argon ion and atom impact ionization. With the new creation rate of argon ions (*i.e.*, by electron impact ionization, calculated in the second electron Monte Carlo model), the argon ion and atom Monte Carlo model is again calculated. This switch between the Monte Carlo models for electrons and for argon ions + fast argon atoms is repeated until convergence is reached (*i.e.*, when the electron, ion and atom impact ionization rates do not change anymore). This may take tens of iterations, at the high voltage under consideration here (2 kV; see below).

Subsequently, the creation rate of slow electrons, resulting from the electron Monte Carlo model (*i.e.*, the transfer rate to the slow electron group), and the creation rate of argon ions, resulting from the electron and ion+atom Monte Carlo models (*i.e.*, the electron, fast argon ion and atom impact ionization rates), are used as inputs in the fluid model. This yields new electric field distributions, as well as new ion fluxes bombarding the cathode and entering the CDS from the NG. This information is again put into the Monte Carlo models. The whole procedure is repeated until final convergence is reached (*i.e.*, generally after 3–7 iterations, depending on the choice of the initial conditions). The whole calculation procedure takes several days on a Digital professional workstation, at a clock speed of 500 MHz and approximately 1 GB RAM.

## 3. Results and discussion

### 3.1. Electrical characteristics

The calculations are performed for typical experimental conditions used in a μs-pulsed Grimm-type glow discharge

source,[76] *i.e.*, a 10 μs pulse with a repetition frequency of 200 Hz, an argon gas pressure of 3 Torr, and an applied pulse voltage of about 2 kV. The Grimm-type source under consideration is assumed to be a simple cylinder, with dimensions of 4 mm diameter and 2.6 cm length. It should, however, be mentioned that these dimensions are typical for the pulsed Grimm source used for optical emission spectrometry; the pulsed Grimm-source used for mass spectrometry has a length of only 3.5 mm.[76]

Fig. 1(a) shows the applied voltage as a function of time, for both the experimental value (dashed line) as well as the input voltage in the model (solid line). It rises rapidly at $t=0$, to values of almost 1600 V, and then it increases further linearly to 2000 V at the end of the pulse ($t=10$ μs). Finally, it drops exponentially towards zero, which is practically reached at about 40–50 μs.

When the voltage, gas pressure and temperature are given, the electrical current can be calculated in the model, as the sum of the microscopic fluxes of the charged plasma species (*i.e.*, electrons and ions). Since the current is a macroscopic quantity, which is also measured experimentally, it can, in principle, easily be used to check the validity of the calculation results, by comparison of the calculated and experimental values. The gas pressure was measured in the experimental set-up to be 3 Torr, constant as a function of time. It should, however, be mentioned that rapid variations of the pressure as a function of time, if they exist, can probably not be measured anyhow. In any case, we assume that the gas pressure is indeed constant in time. The gas temperature is not generally measured. However, when the latter quantity was assumed constant in time, the calculated electrical current appeared to remain high during the entire pulse length, *i.e.*, following a similar time-behavior as the applied voltage in Fig. 1(a). Since this calculated current-profile was in strong disagreement with the experimental time-profile [see below, Fig. 1(b)], this was an indication that the gas temperature had to be a function of time. Again, even if the gas temperature had been measured experimentally, rapid variations as a function of time would probably be difficult to detect. Nevertheless, based on the above consideration, we have assumed in our model that the gas temperature varies as a function of time (see below). From the ideal gas law follows that $p=\frac{n}{V}\mathrm{k}T_\mathrm{g}$, where $p$ is the gas pressure, $n/V$ is the gas density, k is the Boltzmann constant and $T_\mathrm{g}$ is the gas temperature. Hence, since p is constant in time and $T_\mathrm{g}$ varies as a function of time, it follows that the gas density will also be a function of time (see below).

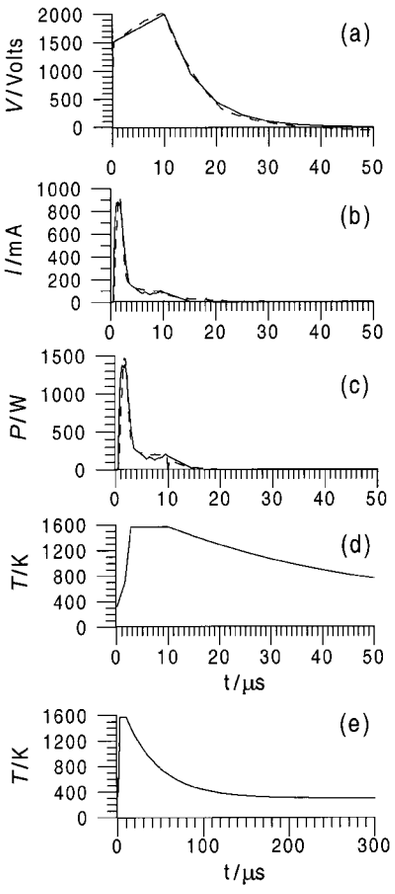


**Fig. 1** Electrical characteristics as a function of time during and after the pulse, at a gas pressure of 3 Torr. The data used as input or calculated in the model are presented by solid lines: (a) applied voltage assumed in the model, (b) calculated electrical current, (c) calculated electrical power, (d) gas temperature assumed in the model, (e) gas temperature assumed in the model, presented at a longer time-scale. The experimental data in (a)–(c) are plotted in dashed lines.

In principle, the gas temperature can be calculated with the heat transfer equation:[77]

$$\rho C_\mathrm{v}\frac{\partial T_\mathrm{g}}{\partial t}-\kappa\frac{\partial^2 T_\mathrm{g}}{\partial \mathrm{z}^2}-\kappa\frac{1}{r}\frac{\partial}{\partial r}\left(r\frac{\partial T_\mathrm{g}}{\partial r}\right)=P$$

where $\rho$ is the gas density, $C_\mathrm{v}$ is the heat capacity at constant volume, $\kappa$ is the thermal conductivity, $T_\mathrm{g}$ is the gas temperature and $P$ is the power input into the argon gas due to collisions of ions, fast atoms and electrons with the argon gas atoms, calculated from Monte Carlo models. In previous work on dc glow discharges, we have used this heat transfer equation, in combination with our Monte Carlo models, to calculate the gas temperature at typical VG9000 and Grimm-type operating conditions.[77] It was found that the gas temperature can rise significantly above room temperature, certainly at high input powers (*e.g.*, at 500 Pa (=3.75 Torr) and 1000 V, a maximum gas temperature of about 1000 K was calculated[77]). However, there are considerable uncertainties in the calculated gas temperature values, since the boundary conditions (especially the temperature at the cathode, but also thermal accommodation coefficients at the cell walls) are not exactly known. On the other hand, it has been mentioned previously[78] that the gas temperature (as well as the gas pressure) is a very critical input parameter in our models, to calculate the electrical current (and other related quantities like plasma densities and ionization rates), *i.e.*, small variations in the input gas temperature (*e.g.*, 30%) yielded large variations (*i.e.*, a factor of 2) in the calculated current,[78] due to a snowball-effect. Indeed, a slightly lower gas temperature at a given pressure yields a correspondingly higher gas density because $\frac{n}{V}=p/\mathrm{k}T_\mathrm{g}$, which gives rise to somewhat more ionization collisions, and hence the creation of more electrons and ions. These extra electrons and ions lead to new ionization collisions, creating more electrons and ions, which give again more collisions, *etc*.

Because of the rather large uncertainties in the gas temperature values calculated with the heat transfer equation (see above), in combination with the considerable effect of this parameter on the calculated electrical current, it was in practice not feasible to use the gas temperature, calculated as a function of time in the heat transfer equation, as input in the present model for the μs-pulsed discharge. Instead, we used the gas temperature as a function of time as a kind of fitting parameter in our model, to calculate a time-variation of the electrical current, which is in agreement with the experimental current–time profile. This assumes, of course, that the measurements of the current as a function of time are accurate. Moreover, as mentioned above, the present model describes only the behavior of electrons, argon ions and fast argon atoms, and the excited argon atoms or sputtered cathode atoms and ions are not yet incorporated. This is, however, planned for the near future, and if it is calculated that the cathode ions contribute in a major way to the electrical current, the fitted values of the gas temperature will become somewhat different. Nevertheless, it

should be mentioned that, because small variations in the gas temperature yield large variations in the current, some errors in the experimental or calculated current will not have great effect on the obtained values of the gas temperature.

The gas temperature obtained in this way was then checked against approximate calculations with the heat transfer equation given above, and it appeared that our "fitted" gas temperature as a function of time was indeed realistic (see below). Nevertheless, it should be realized that this fitting of the gas temperature is an approximation in the model, and it would be extremely interesting to compare the fitted values as a function of time with experimental data. Therefore, we hope that the present work will be a motivation for experimentalists to perform gas temperature measurements as a function of time in μs-pulsed discharges.

The gas temperature, calculated in the above described way, is plotted as a function of time in Fig. 1(d) and (e). The time-variation will be explained in more detail below, but it should be kept in mind that this time-varying gas temperature determines, through the time-varying gas density, the calculated electrical current as a function of time. The latter is plotted against time in Fig. 1(b) (solid line), together with the measured value (dashed line). After a short delay, the current appears to increase rapidly to almost 1 A at 1.5–2 μs. After this maximum, the current drops as rapidly to much lower values of about 100 mA at about 3–4 μs. This value is more or less sustained till the end of the pulse at 10 μs, after which the current decreases further to almost zero at 20 μs. Hence, it appears that a more or less "steady state" is reached at about 4 μs after initiation of the pulse.

The product of the applied voltage and the resulting electrical current, yields the electrical power, which is presented as a function of time in Fig. 1c (calculated result: solid line; measured value: dashed line). It shows a similar time-profile as the electrical current, *i.e.*, it reaches a pronounced maximum of nearly 1.5 kW at about 1.5–2 μs, decreases to a steady state value of about 200 W which is maintained from 3–4 μs until the end of the pulse (10 μs), and then drops further to zero at about 15–20 μs. In spite of the very high peak power values, the time-averaged power going into the discharge is rather low, due to the long duty-off time at a 200 Hz pulse repetition frequency (*i.e.*, pulse on: 10 μs; pulse off: 0.005 s − 10 μs = 4990 μs). We calculated a time-averaged power of 0.80 W, which is in agreement with the measured value[77] of 0.78 W, as is of course expected according to the gas temperature fitting approach explained above. This value is much lower than typical power values encountered in dc or rf Grimm-type discharges (order of 10–100 W), but of course the peak power and from that also the plasma densities during the pulse (see below) are much higher than in the dc or rf case.

The gas temperature as a function of time, which yielded the electrical current and power shown in Fig. 1(b) and (c), is presented in Fig. 1(d) and (e). At $t = 0$, there is no power input into the discharge yet, and the gas is at room temperature (300 K). This yields a fairly high gas density, and hence a large amount of ionization, which is responsible for the significant rise in electrical current and (hence) power, observed in Fig. 1(b) and (c).

When the power increases, the gas temperature rises also due to more power input into the gas, first moderately (when the power is not yet very high) and then more drastically (when the power is at its maximum) to values of almost 1600 K at 3 μs. This obtained value was the result of our fitting procedure, but it correlates well with estimations based on the heat transfer equation:

$$\rho C_v \frac{\partial T_g}{\partial t} - \kappa \frac{\partial^2 T_g}{\partial z^2} - \kappa \frac{1}{r}\frac{\partial}{\partial r}\left(r \frac{\partial T_g}{\partial r}\right) = P$$

The power is deposited very quickly, at a time-scale of *ca.* $3 \times 10^{-6}$ s (see below: $dt = dT_g/4.3 \times 10^8$ K s$^{-1}$ and $dT_g = 1600 - 300 = 1300$ K). This is clearly shorter than the characteristic time for heat conduction (see below: $4 \times 10^{-5}$ s). Hence, the heat conduction lags behind, and the 2nd and 3rd terms on the left-hand side can be neglected in first instance. This yields:

$$\frac{\partial T_g}{\partial t} = \frac{P}{\rho C_V}$$

The gas density $\rho (= M/\bar{V})$ is equal to $6.4 \times 10^{-4}$ g cm$^{-3} \times p$ (Torr)/$T$ (K) for argon, and the heat capacity at constant volume $C_v$ is equal to 0.31 J g$^{-1}$ K$^{-1}$. Hence, this yields $\rho C_v = 2 \times 10^{-4}$ J cm$^{-3}$ K$^{-1} \times p$ (Torr)/$T$ (K) $= 7 \times 10^{-7}$ J cm$^{-3}$ K$^{-1}$ at 3 Torr and 850 K [taken as an intermediate value in the temperature rise of Fig. 1(d)]. Further, during the first few microseconds of the pulse, the power density input into the gas, due to collisions of argon ions and fast argon atoms with argon gas atoms, was calculated for the conditions under study here (according to the procedure explained in ref. 77) to be on average of the order of 300 W cm$^{-3}$ (*i.e.*, higher near the cathode, but lower further away from the cathode). Inserting these values of $\rho C_v$ and $P$ into the above equation yields:

$$\frac{\partial T_g}{\partial t} = \frac{300}{7 \times 10^{-7}} \frac{\text{W cm}^{-3}}{(\text{J cm}^{-3}\,\text{K}^{-1})} \cong 4.3 \times 10^8 \text{ K s}^{-1}$$

Hence, the temperature rise is in the order of 430 K per μs during the first few microseconds of the pulse, or about 1300 K in 3 μs: *i.e.*, from 300 K at $t = 0$ to 1600 K at $t = 3$ μs. As a consequence of this high gas temperature (which yields a much lower gas density at a given pressure), the calculated amount of ionization, and hence also the calculated electrical current and power, drop drastically, as is reflected in Fig. 1(b) and (c).

During the remaining time in the pulse, the current and power reach more or less constant values of about 100 mA and 200 W, respectively. We assume that the gas temperature also remains constant at about 1600 K, *i.e.*, there is no further rise in gas temperature, because the power is not extremely high any more (0.2 kW $<<$ 1.6 kW), but there is also no drop in temperature, since the power is still high enough to sustain this high gas temperature. (This can be compared with a kettle of hot water on a low fire that is just high enough to maintain the temperature of the water.) Hence, "steady state" appears to be reached, both for the current, power and gas temperature, starting at about 3–4 μs after initiation of the pulse.

At the end of the pulse (*i.e.*, at 10 μs), the electrical power goes down, and the gas temperature will drop as well. Let us simplify the situation by considering zero input power into the gas, then the gas temperature will decay exponentially according to the characteristic time of heat conduction, $\tau_h = \rho C_V L^2/\kappa$ (ref. 79):

$$T[t - 10(\mu s)] = 300(K) + [T(10\,\mu s) - 300(K)] \times \exp\left(-\frac{t - 10(\mu s)}{\tau_h}\right)$$

At the conditions under study, $\rho C_v \approx 7 \times 10^{-7}$ J cm$^{-3}$ K$^{-1}$ (see above); $\kappa$ is $1.8 \times 10^{-4}$ W cm$^{-1}$ K$^{-1}$ (ref. 77); and $L$ (characteristic diffusion length) is about 0.1 cm. This yields $\tau_h \approx 4 \times 10^{-5}$ s. Hence, this simple estimation predicts that the gas temperature drops exponentially according to a characteristic time of $4 \times 10^{-5}$ s (= 40 μs). This is presented in Fig. 1(d), for 10 to 50 μs (*i.e.*, same time-scale as for the voltage, current and power), and in Fig. 1(e), until 300 μs. This characteristic time of heat conduction is, indeed, large enough to justify the above neglection of the heat conduction term during power deposition. On the other hand, the characteristic time is relatively short compared to the duty-off cycle between the pulses (*i.e.*, 4990 μs for the 200 Hz pulse repetition frequency; see above) so that the gas temperature has enough time to decay back to room temperature before the next pulse starts. Indeed, from Fig. 1(e) it follows that the gas

temperature has almost reached room temperature already at about 200 μs.

This exponential decay of the gas temperature yields again a rise in the gas density, and would therefore lead to a rise in the number of ionization collisions. However, at the same time, the voltage has also dropped exponentially, so that the electrons (and ions and atoms) do not have enough energy anymore to create ionization, and, hence, the electrical current and power return to almost zero.

Since the time-behavior of the electrical characteristics (voltage, current, power) is reasonably well predicted with our model using the fitted gas temperature behavior, we expect that the time-profiles of the other calculated quantities in the model (*e.g.*, densities, ionization rates, *etc*) are also realistic.

### 3.2. Potential distributions at various times

Fig. 2 illustrates the potential distributions throughout the discharge in one dimension (*i.e.*, as a function of distance from the cathode) at various times during and after the pulse. At $t=0$ μs, the initial condition of linear potential drop between cathode and anode was applied in the model, as in a vacuum environment [see Fig. 2(a)]. However, almost immediately after that, the potential drops more steeply from about –1500 V to zero at about 5 mm from the cathode, which is the consequence of the boundary conditions of zero potential at the side-walls (=anode) of the cell. This potential drop remains more or less constant until *ca.* 0.5 μs after initiating the pulse, since the plasma densities are still very low [in correspondence with the low current in Fig. 1(b)]. From now on, however, the plasma densities rise considerably (see also below), and, at 0.6 μs, the potential drops even more rapidly and reaches zero at about 0.5 mm from the cathode [see also Fig. 2(b)]. It has slightly positive values (in the order of 35–40 V) at distances more than 1 mm from the cathode till the end of the discharge cell. This positive value in the negative glow (NG, called the plasma potential) is not only characteristic for pulsed discharges, but is also typical for dc and rf glow discharges. It arises from the fact that a thin sheath is formed at the anode walls (similar to the cathode dark space in front of the cathode, but with a much lower potential drop, in this case 35–40 V), to keep the slow electrons trapped in the plasma.[64] Hence, it appears from Fig. 2 that the glow discharge is clearly burning at 0.6 μs, with a distinct subdivision into a cathode dark space (CDS, from 0 to *ca.* 0.5 mm) and a negative glow (NG, from *ca.* 0.5 mm to the anode).

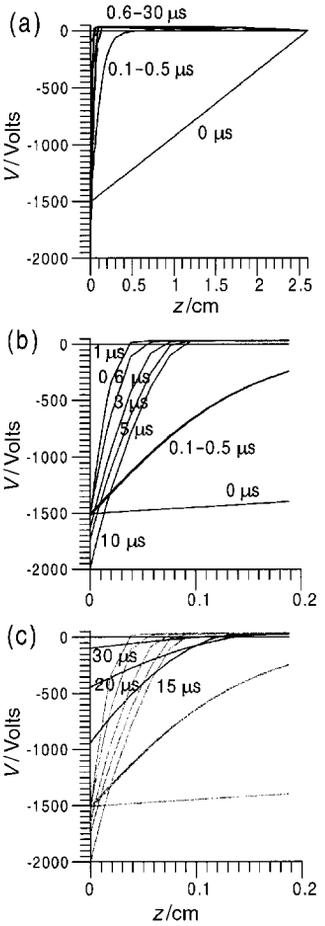


**Fig. 2** Calculated one-dimensional potential distributions at various times during and after the pulse, under the conditions given in Fig. 1, in the entire discharge (a) and in the first 2 mm from the cathode (b) and (c) to show the time-behavior in the CDS in more detail.

The further time-evolution of the potential distribution can be observed more clearly in Fig. 2(b) (at least in the first 2 mm, which represent the CDS and the beginning of the NG). At 1 μs, the potential drops somewhat more steeply from −1500 V at the cathode, to zero at *ca.* 0.3 mm from the cathode. After longer times, until 10 μs, the cathode potential rises more or less linearly to −2000 V, and this larger potential drop (to zero at the end of the CDS) takes place over a slightly larger distance; hence making the CDS somewhat larger, until *ca.* 0.9 mm at 10 μs. The value in the NG (*i.e.*, the plasma potential) remains more or less constant between 35 and 40 V.

At later times [*i.e.*, after termination of the pulse; see bolder lines in Fig. 2(c)], the potential at the cathode decreases exponentially (*i.e.*, *ca.* −950 V at 15 μs; *ca.* −450 V at 20 μs; and *ca.* −100 V at 30 μs), and the potential drop to zero occurs over a somewhat longer distance, giving rise to a more extended CDS. The plasma potential (in the NG) remains of the order of 35–40 V until about 20 μs, but then it drops gradually to zero. Eventually, at about 50 μs, the cathode potential also returns to zero, and hence, the entire discharge is characterized by a zero potential (which corresponds also to the absence of an electric field), and the glow discharge is extinguished.

### 3.3. Plasma densities at various times

Fig. 3(a) and (b) present the calculated densities of argon ions as a function of distance from the cathode, at various times during and after the pulse. The density is very low until *ca.* 0.5 μs. Then it increases rapidly up to a maximum of about $4.5\times10^{14}$ cm$^{-3}$ at 1.5 μs after initiating the pulse [see Fig. 3(a)]. At later times, the density drops again to a value of about $4\times10^{13}$ cm$^{-3}$ at 5 μs [see Fig. 3(b)]. This value is more or less maintained until the end of the pulse (=10 μs). After termination of the pulse, the density decreases further, and it becomes negligible at about 20 μs [see Fig. 3(b)]. This time evolution is very similar to the time-behavior of the calculated electrical current [see above; Fig. 1(b)], which is as expected, since the argon ion density and electrical current are closely related (*i.e.*, the current is calculated from the argon ion and electron fluxes, and the latter are proportional to the argon ion and electron densities).

The density profiles calculated at the various times are all very similar in shape, *i.e.*, the density is low and rather constant in the CDS and reaches a maximum at about 1–3 mm from the cathode (this position shifts slightly to higher values as a function of time), after which it drops again to low values at about 2 cm from the cathode. The electron density is almost identical to the argon ion density (which is necessary in order to have charge neutrality), except that it is zero in the CDS, giving rise there to a positive space charge, and hence, a large potential drop (see also Fig. 2).

### 3.4. Ionization and recombination rates

The ionization rates, due to electron, fast argon ion and atom impact, are characterized by nearly the same time-behavior as

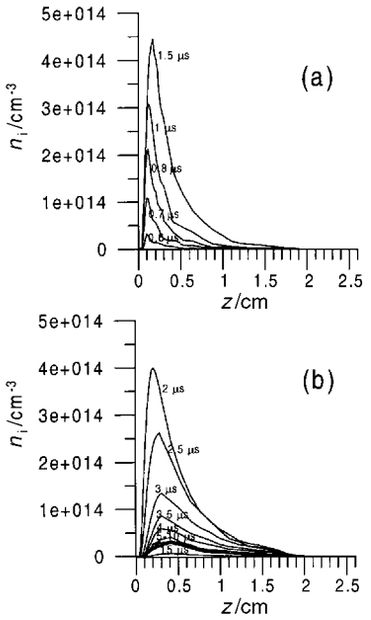


**Fig. 3** Calculated one-dimensional argon ion density profiles at various times during (a) and after (b) the pulse, under the conditions given in Fig. 1.

the argon ion density shown above, and are therefore not presented here at all times. Fig. 4(a) illustrates the electron, ion and atom impact ionization rates, as well as the slow electron creation rate (dashed line) at 2 μs (which is about the maximum in the time evolution).

The electron impact ionization rate reaches a maximum of about $3 \times 10^{20}$ cm$^{-3}$ s$^{-1}$ at 2 mm from the cathode (*i.e.*, in the beginning of the NG), and then it drops gradually to low values at the end of the discharge cell. The slow electron creation rate (dashed line) is zero in the CDS, since there are no slow electrons created here (*i.e.*, slow electrons would not remain slow here, due to the rapid acceleration in the strong electric field). However, it reaches a pronounced maximum of *ca.* $6 \times 10^{20}$ cm$^{-3}$ s$^{-1}$ in the beginning of the NG (at about 2 mm), where the electric field is rather weak, and the electrons are not subject to considerable acceleration anymore. After this pronounced maximum, the slow electron creation rate drops

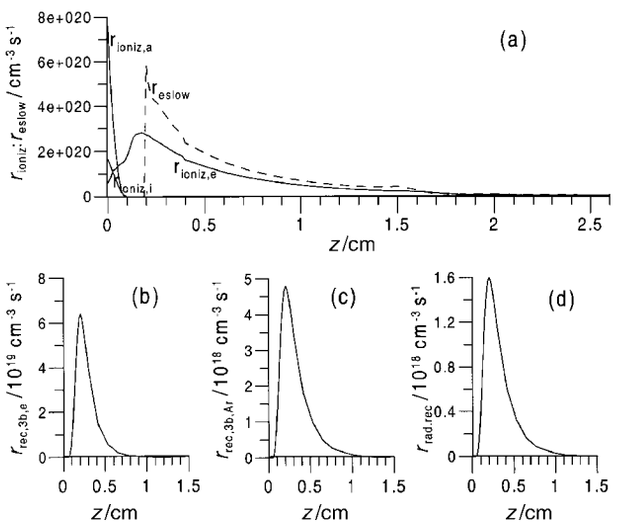


**Fig. 4** Calculated one-dimensional electron, fast argon ion and atom impact ionization rates ($r_{ioniz,e}$ ; $r_{ioniz,i}$ ; $r_{ioniz,a}$) and slow electron transfer rate ($r_{eslow}$; dashed line) (a); and recombination rates, by three-body recombination with an electron as third body ($r_{rec,3b,e}$ (b)), three-body recombination with an argon atom as third body ($r_{rec,3b,Ar}$ (c)), and radiative recombination ($r_{rad.rec}$ (d)), at 2 μs after the start of the pulse. Note that the *x*-axis in Fig. (b)–(d) is truncated at 1.5 cm.

exponentially, and it becomes similar to the electron impact ionization rate at about 1 cm from the cathode. Hence, in the bulk of the NG, every ionization collision appears to yield the formation of a slow electron.

The fast argon ion and atom impact ionization rates at 2 μs are also plotted in Fig. 4(a), as a function of distance from the cathode. These processes play a role in the CDS only, and especially adjacent to the cathode, where the argon ions and atoms reach high enough energies. It should, indeed, be mentioned that the cross sections for these processes increase with rising energy. The argon ion impact ionization rate was found to reach a maximum at the cathode of almost $2 \times 10^{20}$ cm$^{-3}$ s$^{-1}$, whereas the maximum argon atom impact ionization rate amounts to $8 \times 10^{20}$ cm$^{-3}$ s$^{-1}$. Hence, these values are of the same order of magnitude as the electron impact ionization rate, which illustrates that the contribution of these processes to the overall ionization of the argon atoms is not negligible.

We have also calculated the argon ion–electron recombination rates due to three-body recombination with the third body being an electron (rec,3b,e) or an argon gas atom (rec,3b,Ar) or radiative recombination (rad.rec). The results are depicted at $t = 2$ μs, as a function of distance from the cathode in Fig. 4(b), (c) and (d), respectively. It is clear that three-body recombination with the third body being an electron is the dominant recombination process at 2 μs (*i.e.*, maximum rate of *ca.* $6 \times 10^{19}$ cm$^{-3}$ s$^{-1}$). Three-body recombination with an argon atom as third body is about one order of magnitude less important (rate of about $5 \times 10^{18}$ cm$^{-3}$ s$^{-1}$ at its maximum), and radiative recombination is still a factor of 3 less important (rate of about $1.6 \times 10^{18}$ cm$^{-3}$ s$^{-1}$). The one-dimensional rate profiles are similar to the argon ion and electron density distributions, but since they are the product of electron and ion densities, they are more peaked at the maximum and drop more rapidly as a function of distance (note that the *x*-axis is truncated at 1.5 cm from the cathode). This is most pronounced for the three-body recombination rate with an electron as the third body, since this rate is proportional to the electron and argon ion densities to the third power (see above, in section 2.2).

When comparing the ionization and recombination rates [*i.e.*, Fig. 4(a) with Fig. 4(b), (c) and (d)], it is clear that ionization is much more important than recombination, which corresponds to our previous observations for a dc discharge (see *e.g.*, ref. 78).

The various ionization and recombination rates, integrated over the entire discharge volume, are presented as a function of time in Fig. 5. There is virtually no ionization until 0.5 μs. This follows, of course, from the above results, *i.e.*, there is almost no electrical current in the first 0.5 μs after initiating the pulse [see the calculated and experimental data in Fig. 1(b)], and hence almost no charged particles (electrons, ions) to give rise to ionization. From 0.5 μs on, however, both the electron, argon ion and atom impact ionization rates rise rapidly to a maximum at 1–2 μs after the start of the pulse, in correspondence to the high (calculated and experimental) current. After this maximum, the ionization rate drops slightly as a function of time, but is still considerable at 10 μs (*i.e.*, the end of the pulse). At later times, the ionization rate drops more significantly, since both the applied voltage and the electrical current return to zero. It appears from Fig. 5 that the total electron impact ionization rate (solid line) and the total slow electron transfer rate (dashed line) are more or less equal to each other, which could also be expected from Fig. 4(a), since the areas under the curves are very similar. The argon ion and atom impact ionization rates, integrated over the entire discharge volume, are clearly lower than the electron impact ionization rate; these processes are important only very close to the cathode. Nevertheless, it will be shown later that their

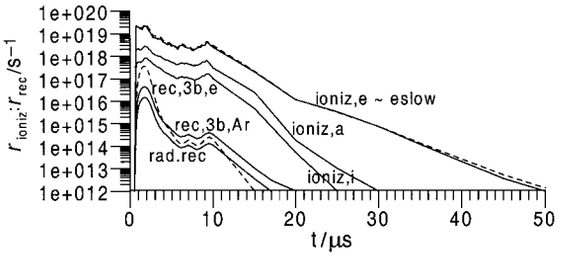


**Fig. 5** Calculated ionization rates, slow electron transfer rate and recombination rates by the various mechanisms indicated in Fig. 4, integrated over the entire discharge volume, as a function of time during and after the pulse.

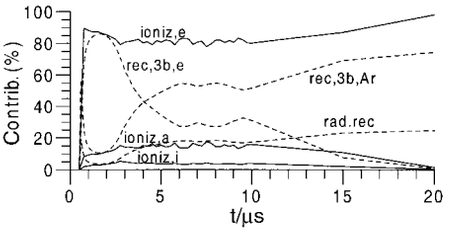


**Fig. 6** Calculated relative contributions of the various ionization (solid lines) and recombination (dashed lines) mechanisms indicated in Fig. 4, integrated over the entire discharge volume, as a function of time during and after the pulse.

relative contributions to the overall ionization are not negligible.

The calculated recombination rates, integrated over the entire discharge volume, are also plotted against time in Fig. 5. They are also virtually zero until 0.5 μs, which is logical since the argon ion and electron densities are very low here. The overall recombination rates appear to be clearly lower than the ionization rates, which is a consequence of the lower rates at the maximum, and also the more pronounced drop as a function of distance [see Fig. 4(b)–(d)]. Moreover, it appears from Fig. 5 that the recombination rates decrease more rapidly as a function of time than the ionization rates, because they result from the product of electron and ion densities, which both decrease as a function of time. This drop is most significant for three-body recombination with an electron as third body (rec,3b,e; dashed line) since it is proportional to the electron/argon ion densities to the third power. At the end of the pulse (10 μs), it appears that recombination is clearly lower than ionization. This is rather unexpected, since it is stated in the literature (*e.g.*, refs. 17,19) that the metastable density peaks at the end of the pulse in millisecond pulsed discharges, probably due to the formation by electron–ion recombination. However, the result we obtained here seems also logical, *i.e.*, the recombination decreases due to a drop in the argon ion and electron densities, and the latter are directly correlated to the drop in electrical current (see above), which is also experimentally observed. Therefore, we expect that the peak in metastable density is not due to a higher production of electron–ion recombination (which has been found to be a minor production mechanism for the argon metastable atoms at the typical analytical discharge conditions[60]), but rather due to a drop in the loss mechanisms of the metastable atoms. On the other hand, even if there is no drop in the loss processes, we have estimated that the life-time of metastable argon atoms is typically longer than the pulse duration. Indeed, in ref. 80, we found that the total metastable loss rate reached a maximum of about $2 \times 10^{16}$ cm$^{-3}$ s$^{-1}$, for a calculated argon metastable atom density of about $6 \times 10^{11}$ cm$^{-3}$ at its maximum. Hence, the loss rate per metastable atom was about $3.3 \times 10^{4}$ s$^{-1}$. If we define the metastable life-time as being inversely proportional to the loss rate per metastable atom, then we obtain a typical life-time of $3 \times 10^{-5}$ s (or 30 μs). This is, indeed, longer than the pulse duration (*i.e.*, 10 μs). Hence, it is expected that the argon metastable atoms are still present in the plasma when the electrical current, and therefore also the charged plasma species (like argon ions and electrons), have already disappeared (see Figs. 1 and 3). In the near future, we want to investigate in more detail the time-evolution of the metastable argon atoms, by means of our detailed model for the argon excited levels.[80]

Finally, Fig. 6 presents the relative contributions of the various ionization and recombination mechanisms as a function of time. The contributions of the ionization mechanisms (solid lines) are roughly constant in time. It is clear that electron impact ionization is the dominant ionization mechanism (*i.e.*, about 80%). However, the role of fast argon ion and especially fast argon atom impact ionization is not negligible, with a calculated contribution of about 5% and 15%, respectively. This is somewhat higher than that found for a dc glow discharge at similar pressure[81] (*i.e.*, 1–3% and 2–8%, respectively), which is due to the higher pulsed voltage, and hence higher ion and atom energies and therefore more efficient ionization.

The relative contributions of the various recombination mechanisms (dashed lines) appear to vary more significantly with time. In the first few μs of the pulse, three-body recombination with an electron as third body is clearly dominant (>80%), since it is proportional to the electron and ion densities raised to the power of three. However, the contribution of this process decreases clearly when the argon ion and electron densities decrease, and it becomes less important than three-body recombination with an argon atom as third body around 4 μs, and even less important than radiative recombination around 12 μs. In the second half of the pulse (5–10 μs), three-body recombination with an argon atom as third body is the dominant recombination mechanism, with a contribution of about 50%. After termination of the pulse, this value increases up to 60–70%. The contribution of radiative recombination is then about 20%.

## 4. Conclusion

We have developed a hybrid Monte Carlo–fluid model to describe the behavior of electrons, argon ions and fast argon atoms as a function of time, in a μs-pulsed glow discharge. Inputs into the model are the applied voltage as a function of time, as well as the gas pressure. This enables us to calculate the electrical current and power as a function of time. These are compared with experimental data under the same conditions, and good agreement could be reached when the gas temperature was assumed to vary in time as well. This time-evolution of the gas temperature is explained in some detail, because it was not so straightforward and it distinguishes the present model for a pulsed discharge from our previous models for dc and rf discharges, where the gas temperature was assumed constant in time. Moreover, this phenomenon has not yet been described in other papers about pulsed discharges.

Furthermore, the time-behavior of other calculated plasma quantities [such as the electrical potential distribution, the argon ion (and electron) density profiles, and the various ionization and recombination rates, as well as their relative contributions] is also presented in this paper. Although no direct comparison with experimental data was possible for these plasma quantities, we believe that their time-behavior is calculated satisfactorily, because they correlate directly or indirectly to the electrical current, which was found to be in good agreement with the experimental result. In the near future, we would like to extend the present hybrid model to the other (analytically more interesting) plasma species, such as the argon atoms in excited levels (including the metastable atoms), and the sputtered (copper) atoms and ions, in analogy to our dc and rf models, in order to predict their time-behavior as well,

and to check against experimental data. It is, indeed, expected that these species can reach quite high concentrations in the plasma, and they might therefore play a non-negligible role in the pulsed discharge.

## Acknowledgements

A. Bogaerts is indebted to the Flemish Fund for Scientific Research (FWO-Flanders) for financial support. The authors also acknowledge financial support from the Federal Services for Scientific, Technical and Cultural Affairs (DWTC/SSTC) of the Prime Minister's Office through IUAP-IV (Conv. P4/10). Finally, we would like to thank V. Serikov for the interesting and very useful discussions about the time-evolution of the gas temperature; W. Goedheer for his help with the fluid code; and C. Yang and W. Harrison for interesting discussions and supplying the experimental data.

## References

1 J. B. Dawson and D. J. Ellis, *Spectrochim. Acta, Part A*, 1967, **23**, 565.
2 D. G. Mitchell and A. Johansson, *Spectrochim. Acta, Part B*, 1970, **25**, 175.
3 D. G. Mitchell and A. Johansson, *Spectrochim. Acta, Part B*, 1971, **26**, 677.
4 J. F. Kieldopf, *Spectrochim. Acta, Part B*, 1971, **26**, 371.
5 J. O. Weide and M. L. Parsons, *Anal. Lett.*, 1972, **5**, 363.
6 N. Omenetto L. M. Fraser and J. D. Winefordner, *Appl. Spectrosc. Rev.*, 1973, **7**, 147.
7 G. J. Dejind and E. H. Piepmeier, *Anal. Chem.*, 1974, **46**, 318.
8 G. J. Dejind and E. H. Piepmeier, *Spectrochim. Acta, Part B*, 1974, **29**, 159.
9 E. H. Piepmeier and L. de Galan, *Spectrochim. Acta, Part B*, 1975, **30**, 263.
10 T. Araki, T. Uchida and S. Minimi, *Appl. Spectrosc.*, 1977, **31**, 150.
11 A. I. Drobyshev and Y. I. Turkin, *Spectrochim. Acta, Part B*, 1981, **36**, 1153.
12 P. B. Farnsworth and J. P. Walters, *Anal. Chem.*, 1982, **54**, 885.
13 P. B. Farnsworth and J. P. Walters, *Spectrochim. Acta, Part B*, 1982, **37**, 733.
14 B. W. Smith, N. Omenetto and J. D. Winefordner, *Spectrochim. Acta, Part B*, 1984, **39**, 1389.
15 J. A. Klingler, P. J. Savickas and W. W. Harrison, *J. Am. Soc. Mass Spectrom.*, 1990, **1**, 138.
16 M. Glick, B. W. Smith and J. D. Winefordner, *Anal. Chem.*, 1990, **62**, 157.
17 J. A. Klingler, C. M. Barshick and W. W. Harrison, *Anal. Chem.*, 1991, **63**, 2571.
18 C. L. Chakrabarti, K. L. Headrick, J. C. Hutton, Z. Bicheng, P. C. Bertels and M. H. Back, *Anal. Chem.*, 1990, **62**, 574.
19 F. L. King and C. Pan, *Anal. Chem.*, 1993, **65**, 735.
20 C. Pan and F. L. King, *J. Am. Soc. Mass Spectrom.*, 1993, **4**, 727.
21 C. Pan and F. L. King, *Anal. Chem.*, 1993, **65**, 3187.
22 Y. Mei and W. W. Harrison, *Anal. Chem.*, 1996, **68**, 2135.
23 D. C. Duckworth, D. H. Smith and S. A. McLuckey, *J. Anal. At. Spectrom.*, 1997, **12**, 43.
24 R. E. Steiner, C. L. Lewis and F. L. King, *Anal. Chem.*, 1997, **69**, 1715.
25 C. L. Lewis, E. S. Oxley, C. K. Pan, R. E. Steiner and F. L. King, *Anal. Chem.*, 1999, **71**, 230.
26 C. Lewis, F. King, S. Doorn and V. Majidi, Optical emission characterization of a pulsed glow discharge laser ablation system, 2000 Winter Conference on Plasma Spectrochemistry, Ft. Lauderdale, FL, USA, January 2000.
27 W. W. Harrison and W. Hang, *Fresenius' J. Anal. Chem.*, 1996, **355**, 803.
28 D. Pollmann, K. Ingeneri and W. W. Harrison, *J. Anal. At. Spectrom.*, 1996, **11**, 849.
29 W. W. Harrison, W. Hang, X. Yan, K. Ingeneri and C. Shilling, *J. Anal. At. Spectrom.*, 1997, **12**, 891.
30 W. W. Harrison, *J. Anal. At. Spectrom.*, 1998, **13**, 1051.
31 W. Hang, C. Baker, B. W. Smith, J. D. Winefordner and W. W. Harrison, *J. Anal. At. Spectrom.*, 1997, **12**, 143.
32 W. Hang, W. O. Walden and W. W. Harrison, *Anal. Chem.*, 1996, **68**, 1148.
33 W. O. Walden, W. Hang, B. W. Smith, J. D. Winefordner and W. W. Harrison, *Fresenius' J. Anal. Chem.*, 1996, **355**, 442.
34 X. Yan, W. Hang, B. W. Smith, J. D. Winefordner and W. W. Harrison, *J. Anal. At. Spectrom.*, 1998, **13**, 1033.
35 K. Ingeneri and W. W. Harrison, Evaluation of laser sampling into the microsecond pulsed glow discharge, Pittsburgh Conference, Orlando, Fl, USA, March 1999.
36 K. Ingeneri and W. W. Harrison, Pulsed laser ablation into a microsecond pulsed glow discharge, FACCS, Vancouver, B.C., USA, October 1999.
37 C. Yang, K. Ingeneri and W. W. Harrison, *J. Anal. At. Spectrom.*, 1999, **14**, 693.
38 A. Bengtson, C. Yang and W. W. Harrison, Microsecond pulsed glow discharge optical emission spectrometry—Investigation of temporal emission characteristics, 2000 Winter Conference on Plasma Spectrochemistry, Ft. Lauderdale, FL, USA, January 2000.
39 E. Oxley, C. Yang and W. W. Harrison, Sputter rates in μs-pulsed glow discharge atomic emission spectrometry, 2000 Winter Conference on Plasma Spectrochemistry, Ft. Lauderdale, FL, USA, January 2000.
40 C. Yang, M. L. Mohill and W. W. Harrison, Grimm-type glow discharge ion source for time-of-flight mass spectrometry, 2000 Winter Conference on Plasma Spectrochemistry, Ft. Lauderdale, FL, USA, January 2000.
41 W. W. Harrison and W. Hang, *J. Anal. At. Spectrom.*, 1996, **11**, 835.
42 W. Hang, P. Yang, X. Wang, C. Yang, Y. Su and B. Huang, *Rapid Commun. Mass Spectrom.*, 1994, **8**, 590.
43 Y. Su, Z. Zhou, P. Yang, X. Wang and B. Huang, *Spectrochim. Acta, Part B*, 1997, **52**, 633.
44 Y. Su, P. Yang, Z. Zhou, X. Wang, F. Li, B. Huang, J. Ren, M. Chen, H. Ma and G. Zhang, *Spectrochim. Acta, Part B*, 1997, **53**, 1413.
45 P. Yang, Y. Su, Z. Zhou, X. Wang, F. Li and B. Huang, *Anal. Sci.*, 1997, **13**, 3.
46 C. Lewis, G. Jackson, F. King, S. Doorn, V. Majidi and D. Wayne, Temporally and spatially resolved diagnostics of a pulsed glow discharge source, 2000 Winter Conference on Plasma Spectrochemistry, Ft. Lauderdale, FL, USA, January 2000.
47 R. E. Steiner, C. L. Lewis and V. Majidi, *J. Anal. At. Spectrom.*, 1999, **14**, 1537.
48 V. Majidi, M. Moser, C. Lewis, W. Hang and F. L. King, *J. Anal. At. Spectrom.*, 2000, **15**, 19.
49 V. Majidi, W. Hang, M. Moser, C. Lewis and F. King, Complete chemical speciation by low pressure tunable plasmas, 2000 Winter Conference on Plasma Spectrochemistry, Ft. Lauderdale, FL, USA, January 2000.
50 M. Moser, C. Lewis, F. L. King, W. Hang and V. Majidi, Acquisition of elemental, structural and molecular information using microsecond pulsed glow discharge, 2000 Winter Conference on Plasma Spectrochemistry, Ft. Lauderdale, FL, USA, January 2000.
51 A. Bogaerts, R. Gijbels and W. J. Goedheer, *J. Appl. Phys.*, 1995, **78**, 2233.
52 A. Bogaerts, R. Gijbels and W. J. Goedheer, *Anal. Chem.*, 1996, **68**, 2296.
53 A. Bogaerts, R. Gijbels and W. J. Goedheer, *Jpn J. Appl. Phys.*, 1999, **38**, 4404.
54 A. Bogaerts, M. Yan, R. Gijbels and W. J. Goedheer, *J. Appl. Phys.*, 1999, **86**, 2990.
55 A. Dengra, J. Ballesteros, M. A. Hernandez and V. Colomer, *J. Appl. Phys.*, 1990, **68**, 5507.
56 J.-P. Boeuf and L. C. Pitchford, *IEEE Trans. Plasma Sci.*, 1991, **19**, 286.
57 H. B. Smith, C. Charles, R. W. Boswell and H. Kuwahara, *J. Appl. Phys.*, 1997, **82**, 561.
58 Y. K. Shin, C. H Shon, W. Kim and J. K. Lee, *IEEE Trans. Plasma Sci.*, 1999, **27**, 1366.
59 A. A. Ganeev, V. S. Vergizova, M. V. Voronov, M. N. Slyadnev, S. E. Sholupov and A. A. Stroganov, Glow discharge pulse ionization of residue in thin-walled metallic hollow cathode with time-of-flight mass spectrometry. Experimental and modeling investigation, 2000 Winter Conference on Plasma Spectrochemistry, Ft. Lauderdale, FL, USA, January 2000.
60 A. Bogaerts and R. Gijbels, *Phys. Rev. A*, 1995, **52**, 3743.
61 A. Bogaerts and R. Gijbels, *J. Appl. Phys.*, 1996, **79**, 1279.
62 A. V. Phelps and Z. Lj. Petrovic, *Plasma Sources Sci. Technol.*, 1999, **8**, R21.
63 A. Bogaerts, M. van Straaten and R. Gijbels, *Spectrochim. Acta, Part B*, 1995, **50**, 179.
64 B. Chapman, *Glow Discharge Processes*, Wiley, New York, 1980.

65 R. van de Sanden, PhD Dissertation, Eindhoven University of Technology, 1991.
66 V. S. Vorob'ev, *Plasma Sources Sci. Technol.*, 1995, **4**, 163.
67 H. S. W. Massey and E. H. S. Burhop, *Electronic and Ionic Impact Phenomena*, Oxford University Press, Oxford, 1952.
68 M. A. Biondi, *Phys. Rev.*, 1963, **129**, 1181.
69 J. D. P. Passchier and W. J. Goedheer, *J. Appl. Phys.*, 1993, **74**, 3744.
70 J.-P. Boeuf, *Phys. Rev. A*, 1987, **36**, 2782.
71 H. K. Gummel, *IEEE Trans. Electron. Devices*, 1964, **11**, 455.
72 D. L. Scharfetter and H. K. Gummel, *IEEE Trans. Electron. Devices*, 1969, **16**, 64.
73 A. V. Phelps, *J. Appl. Phys.*, 1994, **76**, 747.
74 A. V. Phelps, *J. Phys. Chem. Ref. Data*, 1991, **20**, 557.
75 H. Oechsner, *Phys. Rev. B*, 1978, **17**, 1052.
76 W. W. Harrison and C. Yang, private communication.
77 A. Bogaerts, R. Gijbels and V. V. Serikov, *J. Appl. Phys.*, 2000, **87**, 8334.
78 A. Bogaerts, PhD Dissertation, University of Antwerp, 1996.
79 V. V. Serikov and K. Nanbu, *J. Appl. Phys.*, 1997, **82**, 5948.
80 A. Bogaerts, R. Gijbels and J. Vlcek, *J. Appl. Phys.*, 1998, **84**, 121.
81 A. Bogaerts and R. Gijbels, *Spectrochim. Acta, Part B*, 1998, **53**, 437.